



## Bioactive coating provides antimicrobial protection through immunomodulation and phage therapeutics

Kenny Zhuoran Wu<sup>a,1</sup>, Zhicheng Le<sup>a,b,1</sup>, Ba Myint<sup>a,b</sup>, Brian Chan<sup>a</sup>, Ling Liu<sup>b</sup>, Hua Huang<sup>d,e,f</sup>, Swee Leong Sing<sup>c,g</sup>, Andy Tay<sup>a,b,c,\*</sup>

<sup>a</sup> Department of Biomedical Engineering, College of Design and Engineering, National University of Singapore, 119276, Singapore

<sup>b</sup> Institute for Health Innovation & Technology, National University of Singapore, 117599, Singapore

<sup>c</sup> NUS Tissue Engineering Program, National University of Singapore, 117510, Singapore

<sup>d</sup> Department of Physiology, Yong Loo Lin School of Medicine, National University of Singapore, 117597, Singapore

<sup>e</sup> Electrophysiology Core Facility, Yong Loo Lin School of Medicine, National University of Singapore, 117456, Singapore

<sup>f</sup> Healthy Longevity Translational Research Program, Yong Loo Lin School of Medicine, National University of Singapore: Level 5, Centre for Life Sciences, 28 Medical Drive, 117456, Singapore

<sup>g</sup> Department of Mechanical Engineering, College of Design and Engineering, National University of Singapore, 117575, Singapore

### ARTICLE INFO

#### Keywords:

Implant-associated infections

Medical implants

Immune modulation

Bioactive coating

Bacteriophage

### ABSTRACT

Medical implant-associated infections (IAI) is a growing threat to patients undergoing implantation surgery. IAI prevention typically relies on medical implants endowed with bactericidal properties achieved through surface modifications with antibiotics. However, the clinical efficacy of this traditional paradigm remains suboptimal, often necessitating revision surgery and posing potentially lethal consequences for patients. To bolster the existing anti-IAI arsenal, we propose herein a chitosan-based bioactive coating, i.e., ChitoAntibac, which exerts bacteria-inhibitory effects either through immune modulation or phage-directed microbial clearance, without relying on conventional antibiotics. The immuno-stimulating effects and phage-induced bactericidal properties can be tailored by engineering the loading dynamic of macrophage migration inhibitory factor (MIF), which polarizes macrophages towards the proinflammatory subtype (M1) with enhanced bacterial phagocytosis, and Staphylococcal Phage K, resulting in rapid and targeted pathogenic clearance (>99.99%) in less than 8 h. Our innovative antibacterial coating opens a new avenue in the pursuit of effective IAI prevention through immunostimulation and phage therapeutics.

### 1. Introduction

Medical implant-associated infections (IAI) are a significant and severe complication arising from implantation surgeries, contributing to over 100,000 deaths per year in the US [1]. This long-standing clinical issue imposes substantial socioeconomic burdens, manifesting as increased healthcare expenses, additional surgical interventions, prolonged hospital stays, and infection relapse [2,3]. The majority of IAI cases are acute and happen shortly after surgical procedures, which is primarily ascribed to perioperative pathogen infiltration into the implant site, facilitating biofilm formation within a remarkably short timeframe (often <24 h) [4,5]. This means that a tight therapeutic window of ~24 h is essential to combat IAI and prevent it from worsening.

In the event of IAI, the current line of treatment is to administer antibiotics systemically to mitigate pathogenic burdens. While antibiotic therapy is generally effective, its limitations come about when they are unable to reach infection sites and when infections are attributed to multi-drug resistance microbial species. The reported incidence of IAI associated with implants varies across contexts, with rates ranging from 1 to 30% for breast implants [6], 0.4–30% for orthopedic implants [7–9], 1–2% for cardiac implants [10,11], and 0.3–22% for brain implants [12]. Currently, there are medical implants loaded with antibiotics available commercially such as PALACOS® +G\* for local release of antibiotics [13]. Nevertheless, there is increasing worry about the long-term utility and clinical effectiveness of antibiotics, particularly due to observed fitness gains in causative bacteria, such as

\* Corresponding author. Department of Biomedical Engineering, College of Design and Engineering, National University of Singapore, 119276, Singapore.

E-mail address: [bietkpa@nus.edu.sg](mailto:bietkpa@nus.edu.sg) (A. Tay).

<sup>1</sup> These authors contributed equally to this work.

<https://doi.org/10.1016/j.mtbio.2024.101022>

Received 22 December 2023; Received in revised form 7 March 2024; Accepted 9 March 2024

Available online 11 March 2024

2590-0064/© 2024 The Authors. Published by Elsevier Ltd. This is an open access article under the CC BY-NC-ND license (<http://creativecommons.org/licenses/by-nc-nd/4.0/>).

*Staphylococcus aureus* (*S. aureus*) which has led to the emergence of *Methicillin-Resistance Staphylococcus Aureus* (MRSA) [14,15].

In the last two to three decades, significant research endeavors have focused on imparting antimicrobial properties to medical implants. Currently, there are four broad approaches including the use of naturally occurring antimicrobial materials [16,17], incorporation of metal-based nanoparticles [18–24], surface functionalization with antimicrobial peptides (AMPs) [25,26] and surface patterning with high aspect-ratio structures [16,27,28]. Polymers like chitin and chitosan are materials with natural antimicrobial functions [17]. Along with the excellence in antibacterial performance are their desired biodegradability, biocompatibility, minimal cytotoxicity, and excellent physical and chemical properties, making them a good candidate for further modifications to enhance the antibacterial properties [29]. Yet, challenges persist due to a poor understanding of the antibacterial mechanisms and the divergence in efficacy across *in vitro* studies [30].

One other approach involves incorporating metal nanoparticles (Zn, Ag, Cu) into medical implants derived from various materials, including but not limited to titanium (Ti) [18,19], silicone [20,21], polyvinyl chloride [24], latex [22], and stainless steel [23]. Silver-coated medical implants are currently embraced in a diverse range of implantation surgeries [31]. However, the release of cytotoxic ions and the subsequent generation of free radicals from the implants, as the major action principle, might be detrimental to the surrounding healthy tissues with concomitant systemic toxicity, warranting further investigations [32]. Moreover, many bacteria can adapt to and develop resistance to these metal nanoparticles, as evidenced by observed fitness gains reported in many *in vitro* and *in vivo* studies [27]. Notably, in over 100 patient-derived isolates following silver-based anti-infection treatment, *S. aureus* exhibited markedly increased tolerance to silver ions [33]. Considering that most metal elements utilize a similar antibacterial mechanism, it raises concerns on long-term feasibility of relying on metal nanoparticles for IAI prevention.

Alternatively, bactericides with multi-modal antibacterial mechanisms such as AMPs hold promise for reducing selection pressure and enhancing long-term antibacterial efficacy [25,26]. AMPs can be directly grafted onto implants or bound to them with the assistance of nanoparticles, often composed of silicon, poly(glycolic acid) (PGA), poly lactic-co-glycolic acid (PLGA), and chitosan. Despite their known multifaceted antibacterial properties, there exists questions regarding systemic toxicity upon administration. Reports have indicated that certain AMPs, such as colistin, can inflict severe nephrological damage, leading to the suspension of its clinical application [34]. Additionally, AMPs could potentially act as a trigger for bacteria to develop cross-resistance to the innate immune response, particularly the antibacterial response derived from neutrophils [35].

Surface patterning of medical implants with large-aspect-ratio geometries, such as pillars, wires, and tubes, has been reported to provide bactericidal properties [27]. Nevertheless, the efficacy can be heavily influenced by the physical contact of these patterns with bacteria and therefore can be compromised by protein fouling [36]. Furthermore, maintaining high reproducibility and quality for these patterns is another challenge in their clinical translation. This challenge primarily arises from imperfections inherent in current manufacturing technologies, i.e., additive, and subtractive approaches [27].

One aspect that has recently gained increasing traction, yet remains largely underexplored, is leveraging the host's defense system to prevent potential IAI. Among the vast array of the immune system, macrophages play a pivotal role by swiftly accumulating at the site of infection, transforming into proinflammatory M1 subtypes, phagocytizing bacteria, and releasing cytokines that activate other immune cells for controlling infections [37]. Nonetheless, the incorporation of macrophage-modulatory properties into medical implants for the management of IAI, to the best of our knowledge, remains an untapped avenue. Furthermore, the recent revival of interest in phage therapy [38], recognized by the World Economic Forum as one of the top 10

technologies to watch in 2023 [39], offer an alternative antibacterial strategy to conventional antibiotics. Phage therapy uses bacteriophages to target specific pathogenic bacteria and has demonstrated promising results in efficiently eliminating planktonic bacteria and biofilms, even in the presence of strains with multi-drug resistance [40]. Notably, it possesses a remarkable ability to reverse bacterial resistance to antibiotics, which holds potentials for developing an advanced therapy together with the existing spectrum of antibiotics [41].

In this study, we describe a bioactive coating that exploits diverse antimicrobial protection by stimulating either host tissue immunity or through phage therapeutics. Using polydimethylsiloxane (PDMS) as a representative of polymer-based brain-machine interfaces and Ti alloy as a representative metal-based bone repair, we engineered a chitosan-based antibacterial implant coating coined as ChitoAntibac. This coating exerts its antibacterial function by efficient loading and release of macrophage migration inhibitory factor (MIF) or phage K, a bacteriophage against *S. aureus* to control IAI. Specifically, the coating induced polarization of M0 macrophage to pro-inflammatory M1-like phenotype to enhance phagocytosis of bacteria. Additionally, the release of phage K from the coating was also able to achieve rapid and efficient killing of bacteria. Finally, we showed that the coating is biocompatible and non-cytotoxic to neural and bone cells. To the best of our knowledge, this is the first description of a strategy to design a bioactive coating integrating a naturally occurring antimicrobial chitosan material to either stimulate host immune response or provide release of therapeutic phages to leverage on diverse and synergistic protective mechanisms against IAI.

## 2. Materials and methods

### 2.1. Chemicals and organisms

Acetic acid, monochloroacetic acid, N-(3-Dimethylaminopropyl)-N'-ethylcarbodiimide hydrochloride (EDC), N-Hydroxysuccinimide (NHS), 2-(N-Morpholino)ethanesulfonic acid (MES), dopamine hydrochloride, lipopolysaccharides (LPS) from *Escherichia coli* O55:B5, phorbol 12-myristate 13-acetate (PMA), and standard nutrient broth for microorganisms were purchased from Sigma Aldrich. Macrophage migration inhibitory factor (MIF) (#ab75432) and Human MIF ELISA Kit (#ab100594) was obtained from Abcam. PDMS sheets (6" x 8" x 0.04", medical grade) were purchased from BioPlexus. THP-1 cells (human) were obtained from ATCC. Macrophage-SFM (1X) was obtained from ThermoFisher Scientific. Phage K (#19685-B1) and its host strain, i.e., *Staphylococcus (S.) aureus* was obtained from ATCC. Roswell Park Memorial Institute (RPMI) 1640 basal medium was purchased from Gibco. Fetal bovine serum (FBS) was obtained from HyClone.

### 2.2. Synthesis of carboxymethyl chitosan (CMCS)

CMCS was synthesized by carboxymethylation of chitosan following a reported method with modifications [42]. Briefly, 5 g sodium hydroxide was added to the mixture of isopropanol (26 ml) and deionized water (DI H<sub>2</sub>O, 7 ml) at room temperature. The as-prepared solution was then heated to 60 °C and stabilized for at least 0.5 h. Next, 1 g chitosan (medium Mw, #448877 Sigma Aldrich) was slowly added to the solution with vigorous stirring. This alkalization process lasted for 1 h, which was followed by adding isopropanol (7 ml) containing 5 g monochloroacetic acid to the solution. The carboxymethylation reaction continued for another 24 h and then was terminated by adding 1 ml acetic acid. The supernatant was decanted, and the solid parts were resuspended and washed with 70% ethanol for 3 times. The resultant product was then purified by dissolving it into DI H<sub>2</sub>O and subsequently precipitating it by absolute ethanol. The purified and dry CMCS was obtained by lyophilization of the precipitates for 3 days. To vary the degree of substitution (DS) in CMCS, the reaction time (1–24 h) and mass of NaOH (1–9 g) varied for the carboxymethylation reaction.

### 2.3. Degree of substitution (DS)

pH titration was performed to determine the degree of substitution (DS) in CMCS [43]. Briefly, 100 mg CMCS powder with unknown DS was dissolved in 20 ml of 0.1 M HCl and titrated with 0.1 M NaOH at room temperature. NaOH solution was added in portions of 0.05 ml in interval of 20s. The value of pH with the corresponding titrant volumes were recorded and plotted in a graphic to find the inflection points. The DS for various CMCS samples was calculated using the following equation (1):

$$DS = \frac{161A}{m_{CMCS} \cdot 58A} \quad (1)$$

where  $A = V_{NaOH} \times C_{NaOH}$ ;  $V_{NaOH}$  (L) and  $C_{NaOH}$  (M) are the volume and molarity of NaOH titrant;  $V_{NaOH} = \Delta (V_{2^{nd} \text{ inflection point}} - V_{1^{st} \text{ inflection point}})$ ;  $m_{CMCS}$  is the mass of CMCS (g), and 161 and 58 are the molecular weight of glucosamine and a carboxymethyl group, respectively.

### 2.4. Fabrication of polydopamine (PDA)-Coated PDMS/Ti alloy

PDMS sheets were first cut into rectangular pieces with 1 cm in width and 4 cm in length. To prevent surface contamination, the prepared PDMS pieces were immersed in absolute ethanol and washed 3 times in an ultrasonic bath before surface modifications. Dopamine hydrochloride was dissolved in Tris buffer (10 mM, pH 8.5) to obtain the final concentration of 2 mg/ml. Next, the PDMS pieces were submerged into the dopamine hydrochloride solution and the reaction was conducted at room temperature with vigorous stirring. Upon completion of the reaction (8 h), the resultant PDA-coated PDMS samples were rinsed with DI H<sub>2</sub>O 3 times and dried with nitrogen gas. The same protocol was employed for fabrication of PDA-coated Ti alloy ( $d = 0.5 \text{ cm}$ ,  $l = 1 \text{ cm}$ ).

### 2.5. Fabrication of CMCS-coated PDMS/Ti alloy

The as-fabricated PDA-coated PDMS and Ti implants were further surface functionalized with CMCS. CMCS powder was first dissolved in Tris buffer (10 mM, pH 8.5) to obtain the final concentration of 2 mg/ml. The as-fabricated PDA-coated PDMS or Ti alloy was immersed in the CMCS solution, and the reaction was allowed to continue at room temperature with vigorous stirring over different time durations (2, 4, 8, 24, 36, 48 h). To determine whether the CMCS coating was successfully functionalized onto the implant materials and the reaction duration to obtain the equilibrium, contact angle of the resultant products were analyzed by the means of sessile droplet using optical tensiometers (Holmarc).

### 2.6. Fabrication of ChitoAntibac coated PDMS/Ti alloy

Crosslinking of CMCS implant coatings was achieved by the classic EDC/NHS coupling reaction, which initiates covalent bonding between the primary amine (NH<sub>2</sub>) and the carboxylic (COOH) moieties in CMCS. The crosslinking solutions with various concentration of EDC (1, 5, 15, 25, 50 mM) and NHS (NHS: 0.2, 1, 3, 5, 10 mM) at a constant molar ratio ( $v/v = 5:1$ ) were prepared by dissolving the reagents into MES buffer (pH 6). The CMCS-coated PDMS or Ti alloy was immersed in the crosslinking concoctions and allowed to react for 6 h at room temperature with a stirring speed of 200 rpm. The final products were dried with nitrogen gas and kept in a desiccator with silica gels for further use. The PDMS implants post crosslinking were named ChitoAntibac PDMS #1 to #5 depending on the concentration of EDC and NHS used; and larger numbers correspond to the higher concentrations.

### 2.7. Fourier-transform Infrared Spectroscopy

Fourier-transform Infrared Spectroscopy (FTIR) was used to confirm successful surface modification of PDMS sheets with PDA. Briefly,

samples were loaded in the sampling region of the FTIR machine (PerkinElmer) and IR spectra were examined using attenuated total reflectance (ATR) mode. Calibration was carried out prior to sample characterization to remove background noise.

### 2.8. Atomic force microscopy

Atomic force microscopy (AFM) was used to confirm and characterize the surface modification of PDMS substrates with PDA. One-step calibration was performed to ensure proper imaging. The PDA-coated PDMS sheets were loaded onto the sampling region and then examined by AFM (Bruker Dimension Icon AFM) in multiple spots within the frame region in tapping mode using Bruker's SCANASYST-Air commercial cantilever tip which has triangular geometry with 2 nm tip diameter. Raw data were then exported and subjected to further analysis by NanoScope Analysis v1.40.

### 2.9. Loading and release of MIF

The crosslinked PDMS substrates were first processed into  $1 \times 1 \text{ cm}$  and then loading experiments were conducted by immersing the substrates into MIF containing MES solution (1 ml, pH 6). MIF loading was performed at 4 °C with gentle shaking. The loading efficiency as a function of time (0–10 h) was examined to determine the optimal loading duration. Upon reaching each time point, 1  $\mu\text{l}$  of solution was drawn out, diluted by 500 times with MIF ELISA assay buffer, and subjected to MIF quantification using MIF ELISA kit (Abcam 100594). The obtained data was then normalized with pre-established MIF protein standard curve acquired strictly following the vendor's Instruction.

To characterize the release kinetic of MIF from the implant materials, the MIF-laden ChitoAntibac PDMS sheets were submerged into serum-free RPMI 1640 culture medium. MIF release experiments were conducted at 37 °C with gentle shaking. Upon reaching the selected time points, 1  $\mu\text{l}$  of the solution was drawn out for measuring the MIF concentration following the protocol as above, with refill of 1  $\mu\text{l}$  of the culture medium to offset the change in volume.

### 2.10. Macrophage polarization and phagocytosis

Before polarization experiments, resting (M0) macrophages were generated by inducing differentiation of THP-1 cells. THP-1 cells with a cell density of 40,000/cm<sup>2</sup> were suspended in the complete cell culture medium (RPMI 1640 supplemented with 10% FBS and 1% v/v pen/strep) in 6 well plates and treated with 100 nM PMA for 24 h. After the induction process, non-attached cells were removed by aspiration, and adherent cells were washed by PBS to rinse off the PMA excess. The as-obtained M0 macrophages were characterized by counterstaining of M0 markers, i.e., CD 14 and CD 68, and further used for M1 polarization experiments.

To investigate if MIF could induce M1 polarization, M0 macrophages were treated with 800 ng/ml MIF in the complete cell culture medium for 8 h. Lipopolysaccharide (LPS) with a concentration of 100 ng/ml was used as a positive control to validate the M1 polarization by MIF treatment. After the MIF or LPS treatment, the cells were counterstained with a M1 marker (CD 80) to assess their differentiation status. For assessing the effects of MIF-loaded ChitoAntibac PDMS sheets on the polarization of macrophages, the same protocol was applied except that there was a change in the cell culture setting, where cells were cultured in 24 well plates, but the PDMS sheets were placed into hanging inserts to avoid direct contact with the cells.

To assess the effect of MIF on bacterial phagocytosis in macrophages, the FITC-labelled bacteria were inoculated in the well plates containing macrophages (macrophage: bacteria ratio = 1:20) with or without pretreatment of MIF-loaded ChitoAntibac PDMS sheets. The phagocytosis process was allowed to continue for 3 h. After that, the medium was aspirated, and the bacteria excess was removed by ample washing with

PBS. The phagocytosis status was assessed by fluorescence microscopy (Leica DMi1) and raw data were further processed by ImageJ software.

### 2.11. FITC-labelled *S. aureus*

For surface labeling with FITC, bacteria (*S. aureus* and *MRSA*) were obtained from NUS biobank and grown with an initial density of  $1 \times 10^5$ /ml in the broth media for 6 h and collected by centrifugation at 5000g for 5 min. The bacteria pellets (CFU:  $1 \times 10^6$ ) were resuspended in PBS containing 250  $\mu$ g/ml FITC. The FITC labelling reaction was allowed to continue at 4 °C with orbital shaking at a speed of 300 rpm. Finally, bacteria labelled with FITC were washed thoroughly from excessive dye by PBS and stored at -20 °C for further use.

### 2.12. Immunofluorescence staining

Immunofluorescence (IF) staining of macrophage markers was conducted following general IF protocols provided by the markers' supplier. In brief, cells upon completed pretreatment with PMA, LPS, or MIF loaded CMCS crosslinked PDMS substrates were fixed by 4% paraformaldehyde for 15 min at room temperature. Next, the samples were washed by PBS 3 times and non-specific bindings were blocked with 1% bovine serum albumin (BSA) in PBS buffer. After 1 h BSA blocking, mouse anti-human primary antibodies (CD14, CD68, and CD80) were applied to the samples with a dilution factor of 100. Following which, the samples were washed by PBS for 3 times and counterstained with 10  $\mu$ g ml<sup>-1</sup> Hoechst 33342 and goat anti-mouse secondary antibody tagged by Alexa Fluor 488 (1: 200 v/v) for 1h at room temperature in the dark. The samples were then imaged using fluorescence microscope (Leica DMi1) and data analysis was performed using ImageJ software.

### 2.13. Phage K host specificity assay

Phage K was routinely maintained and propagated according to the method previously reported [44]. In brief, the host *S. aureus* (ATCC 19685) was prepared by culturing them in nutrient agar plates overnight at 37 °C to form colonies, and a single colony was swabbed out, transferred into broth medium, allowed to grow for 16 h with gentle shaking (200 rpm) to produce host suspensions.

The host suspension (100  $\mu$ l) was then mixed with 50  $\mu$ l of phage K lysate in a tube, followed by addition of 5 mL of soft agar (nutrient broth supplemented with 0.65% nutrient agar). The resultant concoction was then poured into an agar plate and incubated at 37°C. To harvest Phage K, 5 mL of SM buffer was added to the phage K cultured agar plate and incubated for a further 4 h under gentle shaking. After that, the phage K lysate was collected into a new tube, adding 2% chloroform, and centrifuged at 4000 g for 15 min to remove bacterial debris. Phage K was then sterilized using a 0.22  $\mu$ m filter and kept at 4 °C.

The titer of phage K stocks was assessed by inoculating 10  $\mu$ l of Phage K serial dilutions in the agar plates containing 5 ml soft agar and 100  $\mu$ l *S. aureus*. After incubation at 37 °C for 24 h, the visible plaques in the most concentrated dilution with no overlapping plaques were enumerated to obtain the concentration of phage K (PFU/ml) [45].

To test the host specificity of phage K, 100  $\mu$ l of the host *S. aureus* ( $\sim 10^7$  CFU/ml) was added to 96-well plates, and then 50  $\mu$ l of SM buffer or bacterial phages at 10, 10<sup>2</sup>, 10<sup>3</sup>, 10<sup>4</sup>, 10<sup>5</sup>, 10<sup>6</sup>, 10<sup>7</sup>, 10<sup>8</sup>, and 10<sup>9</sup> PFU/mL were added to each well. The OD600 was measured at pre-determined timepoints (0–900 min) at 37 °C for 16 h with continuous shaking in a microplate reader (Biotek Synergy HT). Upon completion of the experiment, 100  $\mu$ l of the bacteria in each well were plated in agar plates and the colonies after overnight culture were enumerated to obtain the concentration of the live bacteria (CFU/ml).

### 2.14. Loading of bacteriophage

Phage K was loaded into the ChitoAntibac coated PDMS sheets or Ti alloy by incubating the implants with 1 ml phage K ( $1 \times 10^{10}$  PFU/ml) in MES buffer (50 mM MES, pH = 6.0) at 4 °C with gentle shaking for 12 h. To examine the number of phage K loaded into the implants, the implants were submerged into 1 ml PBS for 12 h at 37 °C, and then the phage K titer released from the implants to the solution was measured as described earlier.

### 2.15. Antibacterial efficacy of the phage K-laden PDMS and Ti implants

$1 \times 10^7$  CFU/ml of host *S. aureus* (100  $\mu$ l) was added to 96-well plates. Then, 50  $\mu$ l of the release medium derived from phage K-laden ChitoAntibac PDMS, ChitoAntibac Ti alloy, or  $10^{10}$  PFU/mL of the bacteriophage was added to each well. OD600 was measured at pre-determined timepoints (0–900 min) at 37 °C for 16 h with continuous shaking. Upon completion of the experiment, the bacteria in each well were plated in agar plates and the colonies after overnight culture were enumerated to obtain the concentration of the live bacteria (CFU/ml). Log reduction of live bacteria was calculated based on the below equation:

$$\text{Log reduction} = \log_{10}(\text{A}) - \log_{10}(\text{B})$$

where A is the number of viable bacteria before treatment and B is the number of viable bacteria after treatment.

### 2.16. Cytotoxicity assay

Primary mouse neurons were obtained according to the method previously reported [46], and cultured in polylysine-coated 96-well plates at  $2 \times 10^4$  cell/well supplied with Eagle's minimum essential medium (Invitrogen) supplemented by 10 mM sodium bicarbonate, 10% FBS, 2 mM L-glutamine, 20 mM KCl, 1 mM pyruvate, and 40 mM glucose. Neurons were cultured for 8 days before experiments. MC3T3-E1 was cultured in MEM  $\alpha$  medium (Gibco) supplemented by 10% FBS and 1% antibiotics and seeded in 96-well plates at  $1 \times 10^4$  cell/well and cultured overnight before use. The cell culture medium was removed, and the release medium obtained by incubating ChitoAntibac PDMS/Ti implants, or MIF/phage K-laden ChitoAntibac PDMS/Ti implants in the cell culture medium for 12 h was added to each well, and further incubated for 1, 3, 5, or 7 days. Upon completion of incubation, viability of the two cell types was evaluated by MTT assay following strictly the instructions provided by the vendor and obtained using the below equation:

$$\text{Cell viability} = \frac{\text{Abs}(570 \text{ nm}) \text{ of tested samples}}{\text{Abs}(570 \text{ nm}) \text{ of control}} \times 100\%$$

### 2.17. Statistical analysis

All experiments in this study were carried out in triplicate. Data are presented as the mean  $\pm$  standard deviation (SD). Origin 9 (OriginLab) was used for statistical analysis. Statistical significance was ascertained with either one-way or two-way analysis of variance (ANOVA) Tukey's post-hoc HSD. Statistical differences are indicated with the probability value (*p*-value of <0.05) in the associated text or figure caption.

## 3. Results

### 3.1. Surface characterization of ChitoAntibac PDMS sheets

To create ChitoAntibac coatings on the surface of PDMS sheets, we followed a previously reported protocol with slight modifications [42]

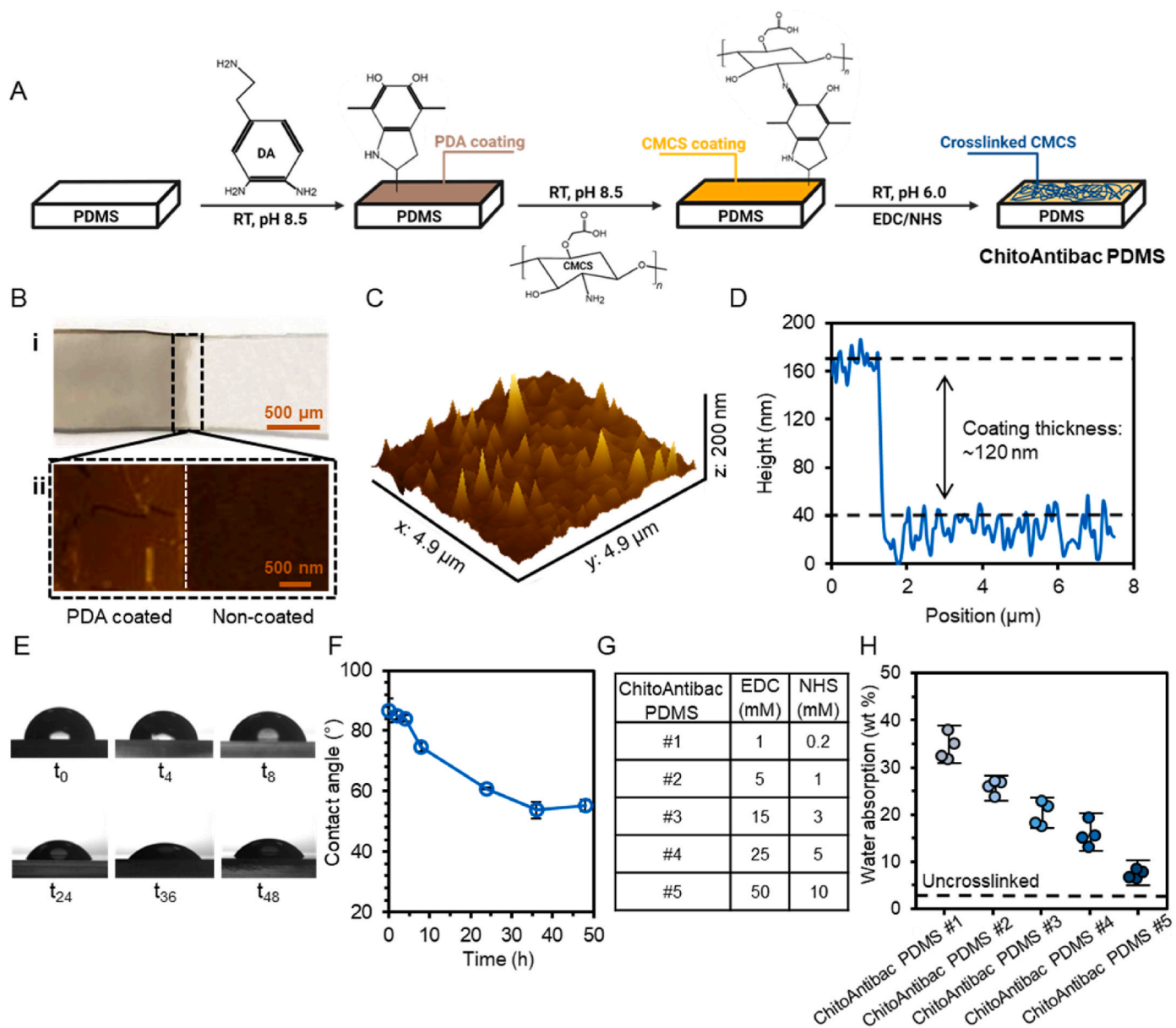


**Fig. 1.** Characterization of PDMS implants with various surface modifications. (A) An illustration of the methodologies for surface modification of PDMS implants. (B) A representative image of the PDMS implants coated with PDA under optical camera (i) with its microstructure at the frame region examined by AFM (ii). (C) A surface topographical image of PDA-modified PDMS implants. (D) A line chart displays the thickness of PDA coating on the PDMS implants with AFM. (E) Contact angle analysis of the hydrophilicity of the PDMS implants subjected to PDA surface modification for various time points. Subscripts under t denote the reaction time. (F) The contact angles for various PDA-coated PDMS implants as a function of reaction time. (G) A computed table summarizes the concentrations of crosslinking agents used for the CMCS crosslinking reactions. (H) The water absorption of ChitoAntibac PDMS sheets crosslinked with various concentrations of EDC and NHS. The dotted line indicates the water absorption of un-crosslinked PDMS sheets.  $n = 4$ . Triplicate experiments were performed unless stated otherwise.

(Fig. 1A). The first step involved enveloping PDMS with a thin uniform layer of polydopamine. The material was exposed to dopamine-containing basic solution (pH 8.5), which provides an oxidation-favored environment for dopamine to initiate spontaneous self-polymerization into polydopamine and subsequently form a firm coating on the PDMS surface through covalent bonds and other intermolecular interactions [47]. ATR-FTIR spectroscopy revealed two distinct peaks that were not present in bare PDMS: a peak at  $3374\text{ cm}^{-1}$  and another at  $1598\text{ cm}^{-1}$ , which are associated with N-H and O-H stretching and N-H bending, respectively, indicating the presence of PDA (Fig. S1). Optical imaging showed desirable evenness of the PDA coatings at the macroscopic scale (Fig. 1Bi) which is further supported with AFM findings at the microscopic level (Fig. 1Bii). Upon analysis of the *in-silico* surface topography reconstruction of the PDA-coated PDMS

sheets, it was found that the average thickness of the coatings was approximately 120 nm (Fig. 1C and D).

After successfully creating a homogenous PDA nanocoating on the silicone materials, the implant surface was modified by conjugating with O-carboxymethylated chitosan (CMCS). CMCS is a natural antibacterial polymeric material with remarkable biocompatibility and was selected in this study to enhance the antibacterial efficacy of the implant coatings. CMCS, derived from chitosan, was synthesized in-house using a previously reported protocol [42]. To achieve the highest degree of carboxymethylation (DOC) in CMCS to impart greater hydrophilicity and negative surface potential for enhancing biofilm inhibition [48], we optimized the reaction conditions, specifically the reaction time and the mass of base salt (NaOH) (Fig. S2). The optimal conditions resulted in a DOC of approximately 80%. To maximize CMCS conjugation onto the

PDA coatings to enhance the wettability of the implant surface, contact angle analysis was carried out which revealed a time-dependent increase in wettability during the CMCS conjugation process, with the lowest angle of  $53^\circ$  observed at the 36-h mark (Fig. 1E and F). In addition, we also noted a distinct yet broader peak spanning from  $1590$  to  $1630\text{ cm}^{-1}$  in CMCS PDMS samples, which is possibly due to the co-existence of N–H and C=O bonds. This is in line with the contact angle analysis, further confirming the successful conjugation of CMCS on the silicone implant surface (Fig. S3). As there was insignificant change in contact angle after 36 h, it likely indicated that the maximal conjugation of carboxymethyl moiety had been achieved.

To create ChitoAntibac implant coatings, the as-obtained CMCS PDMS sheets were further crosslinked using the classic EDC/NHS coupling reaction, which initiates covalent bonding between the primary amine ( $\text{NH}_2$ ) and the carboxylic ( $\text{COOH}$ ) moieties in CMCS [42]. By varying the concentration of crosslinking agents (Fig. 1G), we aimed to create implant coatings with discrepant crosslinking degrees for investigating the impact of the degree of crosslinking on MIF loading capacity of the coatings. We successfully fabricated five ChitoAntibac coatings with distinct crosslinking densities, characterized by marked differences in water retention properties across coatings (Fig. 1H).

Notably, higher concentrations of crosslinkers significantly reduced water absorption and enhanced crosslinking density of the implant coatings.

### 3.2. Loading and release of MIF from ChitoAntibac PDMS

We next evaluated the efficacy of ChitoAntibac coatings in loading macrophage migration inhibitory factor (MIF). MIF is a crucial immunomodulatory mediator involved in various immune responses. It is a member of proinflammatory cytokines that promotes the migration and activation of macrophages. In the human body, one major pathway through which MIF recruits distant macrophages to sites of infection is chemotaxis. One potential method by which MIF can be loaded into the implant coatings involves electrostatic attraction. Considering the variance in the isoelectric point (pI) between MIF (6.23–7.8) and CMCS (5–6), we postulated that MIF loading could be achieved when the pH of the loading solutions falls between 6 and 6.2, causing the two molecules to exhibit opposite surface charges in the solution. To test this hypothesis, MES buffer with a pH of 6 was selected as the loading solution, and MIF loading experiments were conducted with ChitoAntibac PDMS #4 immersed in the MIF-containing loading solution (Fig. S4). We observed

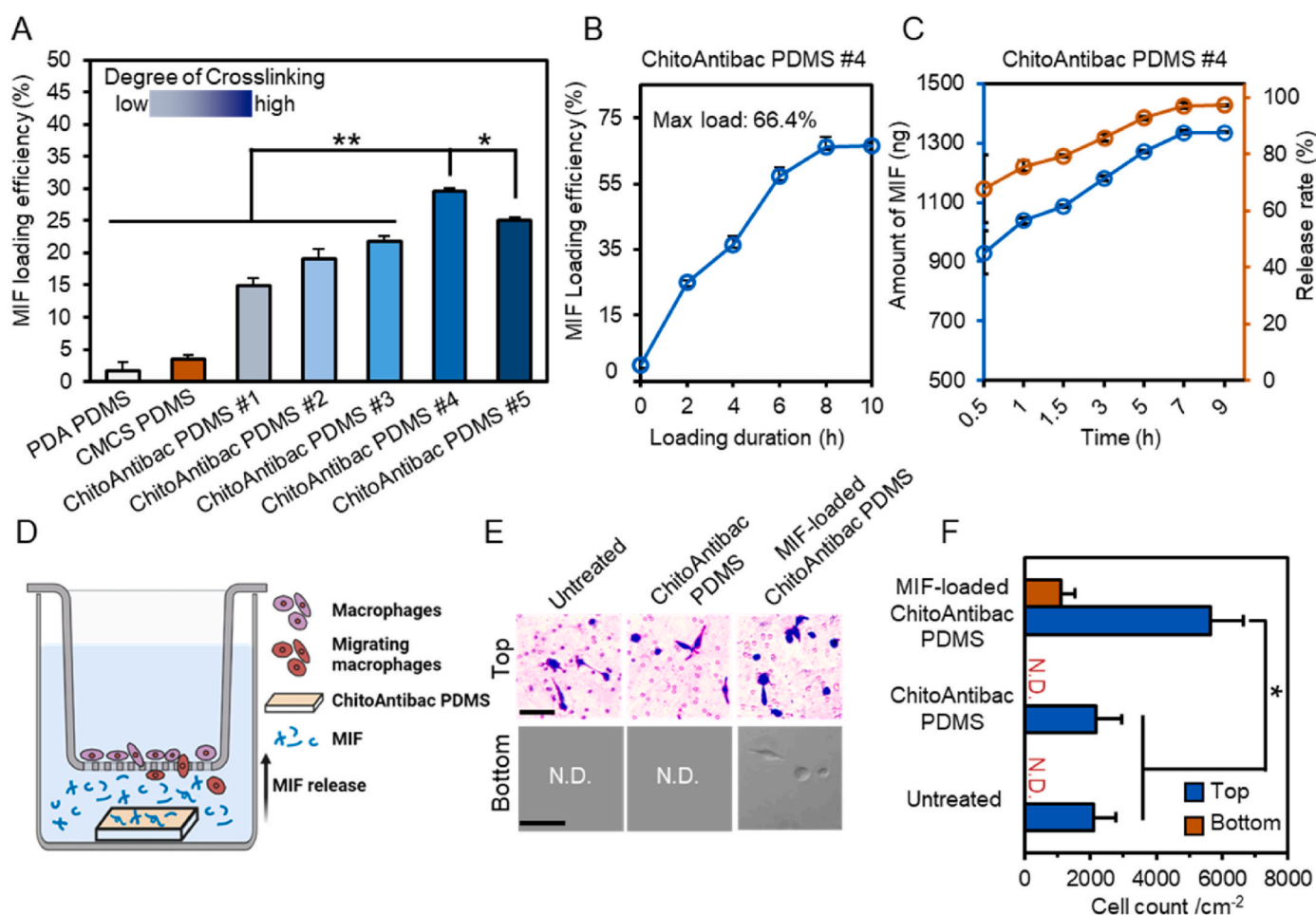


**Fig. 2.** ChitoAntibac PDMS enabled fast release of MIF and induced distant macrophage recruitment. (A) Load efficiency of MIF for ChitoAntibac PDMS implants with various crosslinking conditions was assessed after 2 h of loading. ChitoAntibac PDMS #4 provided the highest MIF loading and therefore was chosen for subsequent experiments. (B) MIF loading efficiency using ChitoAntibac PDMS as a function of time. Maximal loading rate was indicated in the plot. (C) Time-dependent MIF release profile using ChitoAntibac PDMS #4 at physiological temperature ( $37^\circ\text{C}$ ). (D) Schematic illustrating the experimental setup to investigate the effect of MIF released from the ChitoAntibac PDMS implants on macrophage recruitment. (E) Representative images showed macrophage across different groups migrated towards the other side of the inserts or the cell culture well plates after 24 h incubation. Scale bar =  $100\ \mu\text{m}$ . (F) Cell counts of migrated macrophages across different groups. Data are presented as mean  $\pm$  SD. Triplicate experiments were performed. Statistical significance is indicated in the plots where necessary, with \* denotes  $p < 0.05$  and \*\* denotes  $p < 0.01$ .

that nearly 30% of the total input of MIF was loaded into the implants within 2 h (Fig. S5). In contrast, repeating the loading experiments with PBS instead of MES resulted in remarkably lower MIF abundance in the ChitoAntibac coatings. This data supports our hypothesis that MIF could be loaded into the implants through electrostatic attractions.

The impact of crosslinking density on MIF loading was investigated using five different ChitoAntibac coatings as described earlier. As negative controls, PDA PDMS as well as CMCS PDMS exhibited minimal MIF encapsulation (<5%) (Fig. 2A). In stark contrast to the controls, all ChitoAntibac coatings, irrespective of crosslinking density generally demonstrated enhanced MIF loading (>15%) during the 2-h loading experiments. In addition, MIF loading increased with higher crosslinking density. This finding illustrates the crucial role of crosslinked CMCS networks in capturing and retaining MIF within the coatings. Notably, there appeared to be an optimal crosslinking density where the highest MIF loading efficacy was achieved. Beyond condition #4, further increases in crosslinking density led to a decline in MIF loading, possibly due to reduced space for accommodating MIF resulting from increasingly dense CMCS networks. Overall, ChitoAntibac PDMS #4 exhibited the highest MIF loading capacity and was accordingly selected for use in subsequent experiments. For convenience, it would be abbreviated as ChitoAntibac PDMS.

To gain insights into MIF loading kinetics and the maximal loading capacity in ChitoAntibac coatings, loading efficiency was assessed across various timepoints. We noted a time-dependent increase in the loading efficiency, with a maximum at the 8-h mark, representing 66.4% of the total input MIF proteins (Fig. 2B). There was a rapid and efficient release of MIF. Specifically, under physiological conditions, there was a burst discharge of MIF from the implants within the first 0.5 h of the release experiments, followed by a steady and gradual release up to 9 h, at which point all loaded MIF proteins were completely released (Fig. 2C). We argue that this would enable MIF to be therapeutically useful to prevent IAI infection which has a tight therapeutic window of ~24 h before bacterial accumulation.

### 3.3. MIF-loaded ChitoAntibac PDMS recruited and polarized distant macrophages into pro-inflammatory subtypes for enhanced bacterial phagocytosis

To assess whether MIF-loaded ChitoAntibac PDMS can facilitate macrophage migration *in vitro*, resting (M0) macrophages were generated by inducing the differentiation of THP-1 monocytes using phorbol 12-myristate 13-acetate (PMA) (Figs. S6A and B).

As MIF is known to induce macrophages migration and recruit distant macrophages to sites of infection, MIF-loaded ChitoAntibac silicone implants were applied to M0 macrophages in a predetermined transwell setting, allowing the assessment of the MIF effect on cell migration without physical interactions between the implants and the cells (Fig. 2D). The MIF loaded into the implant was allowed to be released by placing the implant onto the surface of well plates and submerging it in compete culture medium. After 24 h, the implants were removed, and cell counting was performed to quantify migrating cells located on the underside of cell culture inserts or bound to well plates. Compared to control, the MIF-laden implant coatings significantly enhanced macrophage migratory activity in both contexts. Specifically, the MIF-containing implant coatings resulted in nearly a 3-fold increase in the number of cells that had migrated to the underside of inserts (Fig. 2E and F). In addition, the release of MIF from the implant coatings also prompted a small population of macrophages to migrate through the inserts' pores, an occurrence undetected in the negative controls. Collectively, these data clearly suggested that MIF-loaded ChitoAntibac implants could stimulate macrophage migration and facilitate their relocation to the implant sites from distant regions.

### 3.4. MIF-loaded ChitoAntibac PDMS sheets activated M1 macrophage polarization and fueled bacterial phagocytosis

A major downstream response of macrophages to MIF stimulation is M1-like subtype polarization, leading to enhanced immunity through a series of important bioprocesses, such as production of proinflammatory cytokine, phagocytosis, and antigen presentation. Consistent with previous findings [49,50], we observed that MIF proteins effectively stimulated M1 polarization, evidenced by a marked increase in the proportion of CD80<sup>+</sup> cells compared to the control (Fig. S7). Considering the maximal amount of MIF that can be loaded into ChitoAntibac implants was approximately 1300 ng (Fig. 2C), we anticipated that applying MIF-loaded implants to M0 macrophages, following the previous transwell setup, would reproduce the observations made with MIF-only treatment. As expected, the release of MIF from ChitoAntibac PDMS sheets induced rapid phenotypic switch in macrophages, resulting in a substantial enrichment of M1 macrophages. These changes were observed as early as 2 h post-treatment (Fig. 3A and B). Through investigating the expression of M1 marker (CD80) over time after the cells interacted with MIF-loaded ChitoAntibac PDMS implants, we noted that MIF induction of macrophage polarization was time-dependent, with the highest level of M1 macrophages at the 6-h mark. Interestingly, there was a gradual weakening of CD80 fluorescence beyond 6 h, suggesting the MIF-induced activation of macrophage polarization was rapid but short-lasting. Although the dynamics of how MIF influences macrophages' immune activity is not completely understood, this observation coincides with previous findings of the potential role of MIF in driving changes in cellular functionalities in a transient fashion [51].

Compared to the naïve form of macrophages (M0), the pro-inflammatory M1-subtype macrophages are equipped with elevated phagocytic capability, enabling more effective bacterial removal at infected implant sites. Therefore, we further investigated whether recruitment and M1 polarization by ChitoAntibac coatings could impart enhanced macrophage phagocytosis. To visualize bacteria during macrophage phagocytosis, we tagged strains of interest (e.g., *S. aureus*) with fluorescein isothiocyanate (FITC) onto their plasma membrane, allowing them to be tracked live under fluorescence microscope (Fig. 3C). Bacterial internalization was detected as early as 3 h across all conditions, suggesting that the stimulation of macrophage phagocytosis holds potential for rapid and efficient control of the early stages of IAI, which typically occur in less than 24 h. Macrophages under unstimulated conditions phagocytized an average of 2 bacteria per cell (Fig. 3D). The release of MIF from ChitoAntibac PDMS sheets led to more than a 2-fold increase in phagocytic capacity. Interestingly, repeating the experiments with MRSA led to a similar observation, characterized by nearly a 3-time greater number of bacteria phagocytized by macrophages upon stimulation by MIF released from ChitoAntibac coatings (Fig. S8). This finding suggests the potential use of ChitoAntibac coatings in dealing with infections stemming from multi-drug resistant bacteria.

### 3.5. ChitoAntibac PDMS/Ti released phage K to rapidly eliminate planktonic bacteria

Recognizing a revived interest phage therapy to manage bacterial infections, we further examined whether our ChitoAntibac coatings could enable medical implants to be integrated with phage therapeutics against IAI. Phage K, known to target specifically *S. aureus*, was selected as a bacteriophage representative, and incorporated into the antibacterial implant coatings using a procedure similar to that for MIF loading. We first established the dose-response profile of phage K at various concentrations over time. As illustrated in Fig. 4A, phage K with concentrations below 10<sup>5</sup> PFU/ml did not exhibit significant suppression of *S. aureus* growth. Conversely, concentrations at or above 10<sup>5</sup> PFU/ml displayed a dose-dependent reduction in bacterial growth, with higher concentrations leading to more pronounced and rapid pathogenic inhibition. Notably, bacterial propagation was nearly completely halted

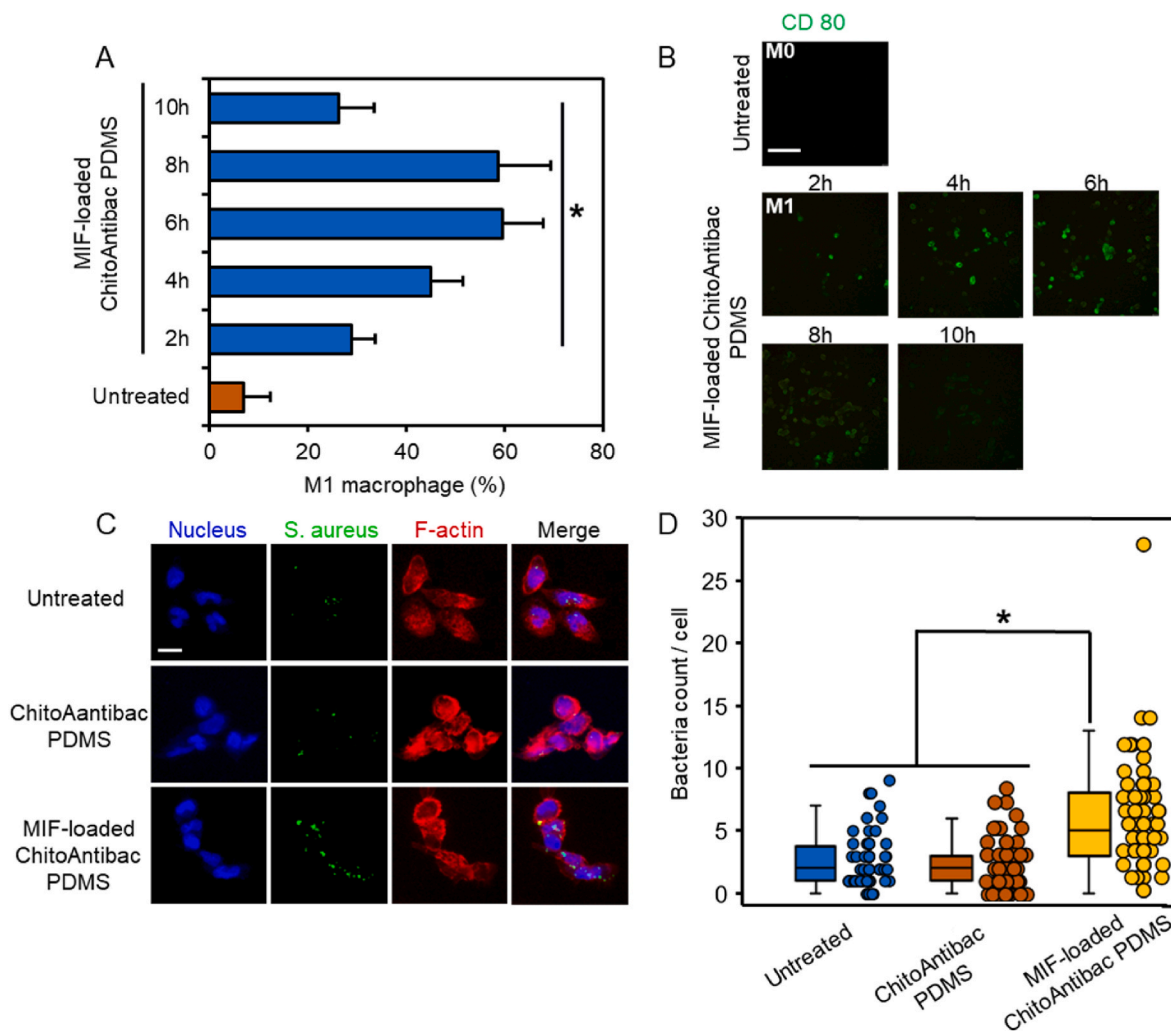


**Fig. 3.** ChitoAntibac PDMS loaded with MIF activated M1 polarization to enhance bacterial phagocytosis. (A) Percent of M1 macrophages after treatment with MIF-loaded ChitoAntibac PDMS for various durations. Quantification of M1 macrophage population was performed by counting cells that had CD 80 expression level more than 2-fold of that of the cells in the control group. (B) Representative fluorescent images showed macrophages stained with CD 80 antibody (green) after treatment with MIF-loaded ChitoAntibac PDMS for various durations. Scale bar = 50  $\mu$ m. (C) Representative fluorescent images showed phagocytosis of *S. aureus* in macrophages with various pretreatments post 3 h of bacterial inoculation. Macrophages were counterstained with Hoechst 33342 (blue) and Phalloidin (red) with the endocytosed bacteria displayed in green. Scale bar = 20  $\mu$ m. (D) Number of *S. aureus* internalized by macrophages with different pretreatments.  $n = 40$ . Triplicate experiments were performed. Statistical significance is indicated in the plots where necessary, with \* denotes  $p < 0.05$ . (For interpretation of the references to color in this figure legend, the reader is referred to the Web version of this article.)

within 9 h. By plotting the bacterial count against phage K concentration with the dose-response data, we determined the minimum inhibitory concentration required for killing 99% of bacteria (MIC99), estimated to be 4.5  $\log_{10}$  PFU/ml (Fig. 4B).

Having identified the effective dose range for phage K, we went on to assess phage K loading capacity of PDMS implants under the same loading conditions as described earlier (MES, pH 6). To validate the broad applicability of our antibacterial coatings for medical implantation, Ti alloy implants with ChitoAntibac coatings were also fabricated and assessed for their capacity to load phage K. ChitoAntibac coatings were able to encapsulate  $> 10^5$  PFU/ml phage K for both PDMS and Ti materials, exceeding the dosage required to achieve MIC99 (Fig. 4C). Motivated by this promising data, we further investigated the impact of phage K-laden coatings on the growth of *S. aureus*.

The release of phage K from the coatings led to rapid (<440 min) and efficient bacterial eradication ( $>7 \log_{10}$ -fold reduction) (Fig. 4D and E). Additionally, we also found that the phage K-loaded PDMS outperformed the Ti alloy in terms of bacteria-eliminating speed (320 vs 440 min), which is likely attributed to the higher loading of phage K in PDMS implants.

### 3.6. ChitoAntibac PDMS/Ti is biocompatible

To evaluate the cytocompatibility of ChitoAntibac-coated implants, we assessed the cytotoxicity of ChitoAntibac PDMS implants on mouse neuron cells, considering the prevalent use of silicone implants in brain-machine interfaces. Additionally, we evaluated the cytotoxicity of ChitoAntibac Ti alloy implants, representing orthopedic implants, on bone cells (MCC3T3-E1). Compared to control, we did not observe any significant reduction in the cell viability of primary neurons caused by MIF or phage K released from the PDMS implants over a 7-day period (Fig. 4F). Similarly, bone cells treated with ChitoAntibac Ti implants for a week remained proliferative and viable, suggesting that the release of MIF and phage K are biocompatible for use in bone implants (Fig. 4G).

## 4. Discussion

Preventing IAI is an unmet clinical challenge, representing a substantial socioeconomic burden and often leading to severe, and sometimes fatal, consequences. The increasing use of medical implantation devices, ranging from bone graft to brain-machine interfaces which have

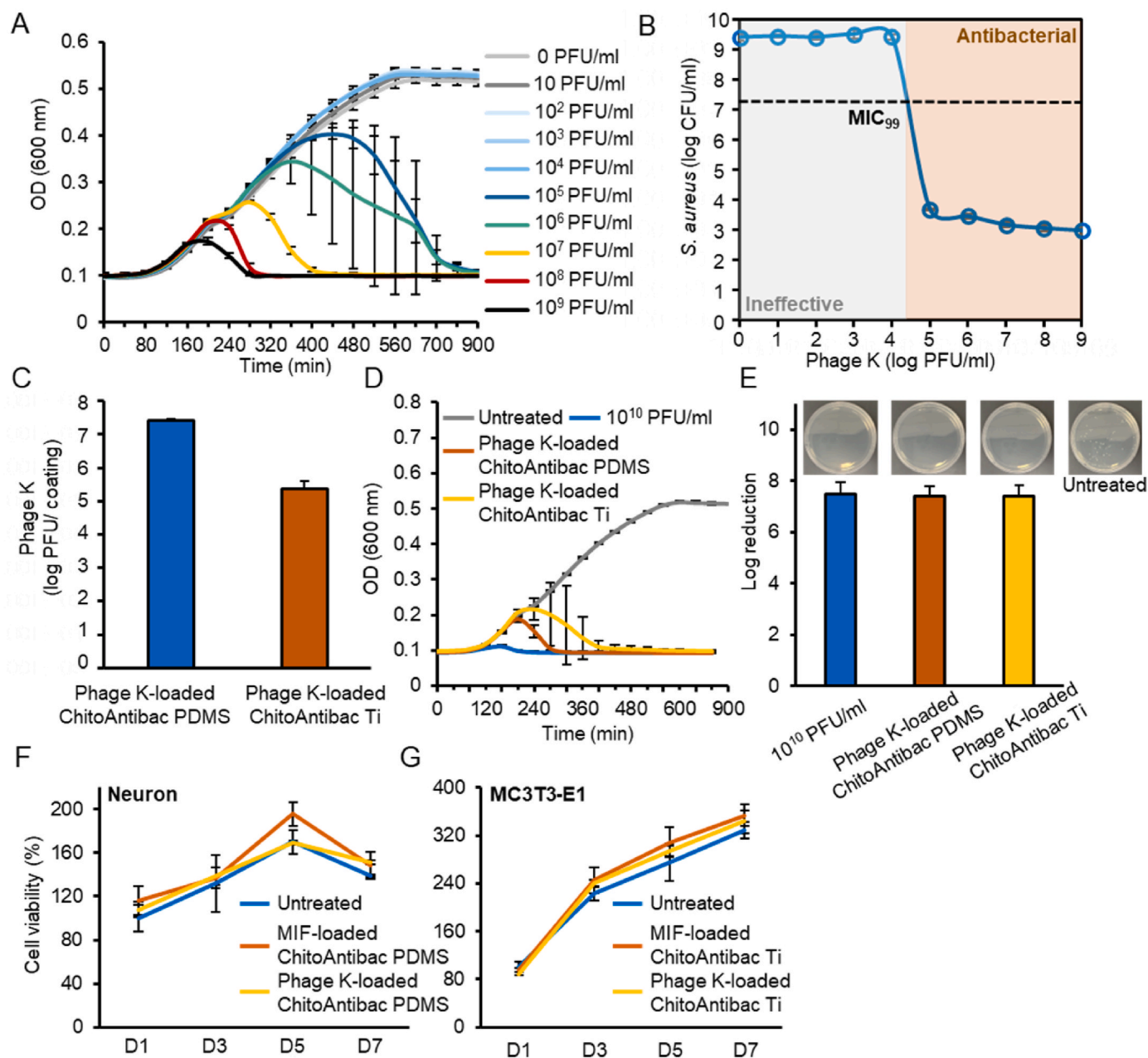


**Fig. 4.** ChitoAntibac PDMS loaded with phage K exhibited rapid and efficient removal of *S. aureus* *in vitro*. (A) Optical density measurement showed dose- and time-dependent bacteria-eliminating property of phage K *in vitro*. (B) Quantification of live bacteria after treatment with different concentrations of phage K. MIC<sub>99</sub> was indicated in the plot and used as a baseline to determine the effective antibacterial dose range (highlighted in light brown). (C) Quantification of phage K loaded into ChitoAntibac coated PDMS sheets and Ti alloy. (D) Optical density measurement shows the antibacterial efficacy of phage-loaded ChitoAntibac PDMS and Ti alloy as a function of time. (E) Log reduction of live bacteria (*S. aureus*) after treatment with ChitoAntibac coated PDMS sheets and Ti alloy. Insets showed optical images of bacterial colonies formed on agar plates that corresponded to respective treatment. (F) Cell viability of mouse neurons after 1-, 3-, 5-, 7-day treatment with ChitoAntibac PDMS loaded with MIF or Phage K. (G) Cell viability of MCCC3T3-E1 bone cells after 1-, 3-, 5-, 7-day treatment with ChitoAntibac Ti loaded with MIF or Phage K. Triplicate experiments were performed. Statistical significance is indicated in the plots where necessary, with \*\* denotes  $p < 0.01$ . (For interpretation of the references to color in this figure legend, the reader is referred to the Web version of this article.)

extended duration in patients' body [52,53], has exacerbated this concern. The standard antibiotic monotherapy only provides moderate effectiveness, and the overuse of antibiotics has contributed to the emergence of advanced bacterial strains like MRSA. This has sparked ongoing debates about the long-term utility of antibiotics against IAI, and the slow development of novel drug classes has further compounded this issue.

Recent efforts in antibacterial strategies for IAI management have focused on developing medical implants without relying on antibiotics.

Current technologies involve (i) surface modifications using bacteria-killing molecules such as antimicrobial peptides (AMPs), metal nanoparticles, or biocompatible polymers with natural antibacterial properties, and (ii) creating large-aspect-ratio surface patterns on the implants *per se*. While these approaches have shown promising antibacterial performance both *in vitro* and *in vivo*, challenges persist, including issues of systemic toxicity, adverse effects on the immune system, manufacturing imperfections, and pathways for bacterial resistance. Our proposed ChitoAntibac implant coating offers a new strategy to treat

implant infections by modulating the innate immune system, specifically macrophage immune response, and leveraging on bacteriophage therapeutics to overcome these existing challenges.

It is crucial to note that most IAIs occur acutely, with biofilm formation on implant surfaces within a day. This provides a fairly short therapeutic window for antibacterial interventions. In our approach, ChitoAntibac coatings were optimized to rapidly release macrophage migration inhibitory factor (MIF) to stimulate distant macrophages' relocation to implant sites, activating M1 polarization within 2 h to enhance immunity against pathogens. *In vitro* examination of macrophage phagocytosis revealed that MIF-stimulated macrophages significantly increased bacteria ingestion as early as 3 h.

On the other hand, the lytic property of phage K is known to induce rapid viral propagation and increase osmotic pressure in the cytoplasm to an overwhelming level where bacterial cells burst to death. Leveraging this unique antibacterial mechanism, the ChitoAntibac coatings encapsulated a sufficient amount of phage K and efficiently (>99.99%) killed planktonic bacteria (*S. aureus*) by releasing loaded phage K in less than 8 h, showcasing their great potential for clinical use in preventing early-stage implant infections and subsequent complications such as biofilm formation.

Carboxymethylated chitosan (CMCS) was chosen as the base material to enhance antibacterial performance of the coating as chitosan has natural antibacterial properties. Optimization of degree of carboxymethylation (DOC) in CMCS and the maximal conjugation of CMCS to the implant coatings contribute to its effectiveness against bacterial adhesion and subsequent biofilm development.

We observed a short-lived effect of MIF to induce macrophage polarization which is consistent with previously established knowledge on the rapid stimulation of macrophage functions by MIF [49]. Our findings are also aligned with previous mechanistic studies attributing transient immune modulation to the dualistic role of MIF in regulating the activity of immune cells and reestablishing homeostasis *in vivo* [51,54,55].

Although the therapeutic use of bacteriophages dates back over a century, the preference for antibiotics has impeded widespread adoption of phage therapy. Recently, a renewed interest in using bacteriophages for infection control arises from growing concerns about pan-antibiotics resistance and the remarkable bacteria-inhibitory effectiveness of phages especially on resistant strains like MRSA [56,57]. However, significantly less attention has been paid to IAI. To the best of our knowledge, we have not seen an example of incorporating phage therapy into medical implants for IAI control. The proposed ChitoAntibac implant coating is a pioneering example, demonstrating superior antibacterial performance in both silicone and Ti alloy implants, holding promise for clinical applications in a wide range of medical implant devices.

Considering the potential development of bacterial resistance to phages over time, future research may focus on constructing phage cocktails containing multiple phages against the same bacterial isolate to reduce selection pressure. Additionally, combining phages and antibiotics may offer a new avenue to restore antibiotic efficacy, and this is achieved by leveraging recent findings on the potential role of phage resistance in reversing bacterial susceptibility to antibiotics. Besides, due to the high phage-host specificity, the use of phage K in our ChitoAntibac coatings is expected to be effective against only *S. aureus*. To resolve this limitation, ongoing research to load multiple phages with distinct hosts into the coatings will broaden the applicability of our proposed strategy to prevent IAI attributing to pathogens beyond *S. aureus*.

While *in vitro* cytotoxicity assessment serves as tentative proof for the biosafety of ChitoAntibac coatings, in the future, *in vivo* tests are necessary to fully reveal the safety profile of this bioactive implant coating. Considering the potential immunological cross-reactivity of phages, these assessments will provide additional insights into the immunotoxicity of phage therapy and justify the clinical use of phage-laden medical implant coatings.

## 5. Conclusion

In this study, we successfully developed an antibacterial implant coating, termed ChitoAntibac, which was incorporated into both silicone and Ti alloy implants. The ChitoAntibac coating permits a facile loading of MIF proteins and phage K, allowing them to be rapidly released under physiological conditions to prevent IAI. The release of MIF proteins induced a prompt activation of macrophage immunity within a few hours, as evidenced by elevated cell migratory activity, an increased proportion of M1 subtypes, and enhanced phagocytosis of bacteria. In addition to the desired immunomodulatory properties, the ChitoAntibac coatings enabled swift release of phage K, resulting in efficient elimination of over 99.99% of *S. aureus* in less than 8 h. This dual functionality of timely immune mediation and bacteria elimination showcases the potential of the coating for clinical applications in controlling early-stage IAI which typically emerges within a day. The biocompatibility of this bioactive implant coating was further evaluated by performing cytotoxicity assay on bone cells and neural cells *in vitro*. Our data tentatively indicates that this implant coating is safe, with no discernible cellular damage. We anticipate that this novel antibacterial implant represents a powerful addition to the existing arsenal against IAI, holding significant potential to enhance the overall well-being of individuals facing IAI.

## Supporting Information

Supporting Information is available from the Elsevier Online Library or from the author.

## CRediT authorship contribution statement

**Kenny Zhuoran Wu:** Writing – review & editing, Writing – original draft, Formal analysis, Conceptualization. **Zhicheng Le:** Writing – review & editing, Writing – original draft, Formal analysis, Conceptualization. **Ba Myint:** Data curation. **Brian Chan:** Data curation. **Ling Liu:** Data curation. **Hua Huang:** Data curation. **Swee Leong Sing:** Data curation. **Andy Tay:** Writing – review & editing, Writing – original draft, Supervision, Conceptualization.

## Declaration of competing interest

The authors declare that they have no known competing financial interests or personal relationships that could have appeared to influence the work reported in this paper.

## Data availability

Data will be made available on request.

## Acknowledgments

The research was supported by NUS Presidential Young Professorship, NUS Technological Innovations Joint Research Grant - October 2020 Infectious Diseases Translational Research Programme (ID TRP) And Health Innovation & Technology (iHealthtech) and National Centre for Infectious Diseases Catalyst Grant.

## Appendix A. Supplementary data

Supplementary data to this article can be found online at <https://doi.org/10.1016/j.mtbio.2024.101022>.

## References

- [1] Y. Hu, et al., Environment-responsive therapeutic Platforms for the treatment of implant infection, *Adv. Healthcare Mater.* 12 (26) (2023) e2300985, <https://doi.org/10.1002/adhm.202300985>.
- [2] I. Potapova, Functional imaging in diagnostic of orthopedic implant-associated infections, *Diagnostics* 3 (4) (2013) 356, <https://doi.org/10.3390/diagnostics3040356>.
- [3] T. Zippelius, et al., Clinical presentation and diagnosis of acute postoperative spinal implant infection (PSII), *J Spine Surg* 6 (4) (2020) 765, <https://doi.org/10.21037/jss-20-587>.
- [4] R. Dower, M.L. Turner, Pilot study of timing of biofilm formation on closed suction wound drains, *Plast. Reconstr. Surg.* 130 (5) (2012) 1141, <https://doi.org/10.1097/PRS.0b013e318267d54e>.
- [5] A. Minkiewicz-Zochniak, et al., Biofilm Formation on dental implant biomaterials by *Staphylococcus aureus* strains isolated from patients with cystic fibrosis, *Materials* 14 (8) (2021), <https://doi.org/10.3390/ma14082030>.
- [6] N.F. Baker, et al., Preventing infection in implant-based breast reconstruction: evaluating the evidence for common practices and standardized protocols, *Plast Reconstr Surg Glob Open* 10 (3) (2022) e4208, <https://doi.org/10.1097/GOX.0000000000004208>.
- [7] O. Camps-Font, et al., Postoperative infections after dental implant placement: prevalence, clinical features, and treatment, *Implant Dent.* 24 (6) (2015) 713, <https://doi.org/10.1097/ID.0000000000000325>.
- [8] M. Ribeiro, et al., Infection of orthopedic implants with emphasis on bacterial adhesion process and techniques used in studying bacterial-material interactions, *Biomater* 2 (4) (2012) 176, <https://doi.org/10.4161/biom.22905>.
- [9] N. Renz, et al., [Osteosynthesis-associated infections : epidemiology, definition and diagnosis], *Unfallchirurg* 120 (6) (2017) 454.
- [10] H.C. Han, et al., Epidemiology of cardiac implantable electronic device infections: incidence and risk factors, *Europace* 23 (23 Suppl 4) (2021), <https://doi.org/10.1093/europace/euab042> iv3.
- [11] M. Malagu, et al., Risk scores for cardiac implantable electronic device infection: which one to believe in? *J. Clin. Med.* 11 (21) (2022) <https://doi.org/10.3390/jcm11216556>.
- [12] A. Conen, et al., Management of neurosurgical implant-associated infections, *Swiss Med. Wkly.* 150 (2020) w20208, <https://doi.org/10.4414/smw.2020.20208>.
- [13] A. Shahid, et al., The prospects of antimicrobial coated medical implants, *J. Appl. Biomater. Funct. Mater.* 19 (2021) 22808000211040304, <https://doi.org/10.1177/22808000211040304>.
- [14] C. Llor, L. Bjerrum, Antimicrobial resistance: risk associated with antibiotic overuse and initiatives to reduce the problem, *Ther Adv Drug Saf* 5 (6) (2014) 229, <https://doi.org/10.1177/2042098614554919>.
- [15] Y.A. Adebisi, Balancing the risks and benefits of antibiotic use in a globalized world: the ethics of antimicrobial resistance, *Glob. Health* 19 (1) (2023) 27.
- [16] R. Bright, et al., Long-term antibacterial properties of a nanostructured titanium alloy surface: an in vitro study, *Mater Today Bio* 13 (2022) 100176, <https://doi.org/10.1016/j.mtbio.2021.100176>.
- [17] M. Haktaniyan, M. Bradley, Polymers showing intrinsic antimicrobial activity, *Chem. Soc. Rev.* 51 (20) (2022) 8584, <https://doi.org/10.1039/d2cs00558a>.
- [18] S. Stein, et al., Osseointegration of titanium implants with a novel silver coating under dynamic loading, *Eur. Cell. Mater.* 39 (2020) 249, <https://doi.org/10.22203/eCM.v039a16>.
- [19] Z. Wang, et al., NanoZnO-modified titanium implants for enhanced anti-bacterial activity, osteogenesis and corrosion resistance, *J. Nanobiotechnol.* 19 (1) (2021) 353, <https://doi.org/10.1186/s12951-021-01099-6>.
- [20] F. Heno, et al., Comparing the antimicrobial effect of silver ion-coated silicone and gentamicin-irrigated silicone sheets from breast implant material, *Aesthetic Plast. Surg.* 45 (6) (2021) 2980, <https://doi.org/10.1007/s00266-021-02348-7>.
- [21] S.R. Sonntag, et al., In vitro evaluation of zinc oxide tetrapods as a new material component for Glaucoma implants, *Life* 12 (11) (2022), <https://doi.org/10.3390/life12111805>.
- [22] D.G. Desai, et al., Silver or nitrofurazone impregnation of urinary catheters has a minimal effect on uropathogen adherence, *J. Urol.* 184 (6) (2010) 2565, <https://doi.org/10.1016/j.juro.2010.07.036>.
- [23] P. Devasconcellos, et al., Antimicrobial particulate silver coatings on stainless steel implants for fracture management, *Mater. Sci. Eng., C* 32 (5) (2012) 1112, <https://doi.org/10.1016/j.msec.2012.02.020>.
- [24] A. Donnadio, et al., PVC grafted zinc oxide nanoparticles as an inhospitable surface to microbes, *Mater. Sci. Eng., C* 128 (2021) 112290, <https://doi.org/10.1016/j.msec.2021.112290>.
- [25] Z. Si, et al., Polymers as advanced antibacterial and antibiofilm agents for direct and combination therapies, *Chem. Sci.* 13 (2) (2022) 345, <https://doi.org/10.1039/d1sc05835e>.
- [26] J. Xuan, et al., Antimicrobial peptides for combating drug-resistant bacterial infections, *Drug Resist. Updates* 68 (2023) 100954, <https://doi.org/10.1016/j.drup.2023.100954>.
- [27] Z. Wu, et al., Microbial resistance to nanotechnologies: an important but understudied consideration using antimicrobial nanotechnologies in orthopaedic implants, *Bioact. Mater.* 16 (2022) 249.
- [28] R. Bright, et al., Bio-inspired nanostructured Ti-6Al-4V alloy: the role of two alkaline etchants and the hydrothermal processing duration on antibacterial activity, *Nanomaterials* 12 (7) (2022), <https://doi.org/10.3390/nano12071140>.
- [29] J. Li, S. Zhuang, Antibacterial activity of chitosan and its derivatives and their interaction mechanism with bacteria: current state and perspectives, *Eur. Polym. J.* 138 (2020), <https://doi.org/10.1016/j.eurpolymj.2020.109984>.
- [30] M.E. Badawy, et al., The antibacterial activity of chitosan products blended with monoterpenes and their biofilms against plant pathogenic bacteria, *Sci. Tech. Rep. (Cairo)* (2016) 1796256, <https://doi.org/10.1155/2016/1796256>, 2016.
- [31] J.M. Schierholz, et al., Efficacy of silver-coated medical devices, *J. Hosp. Infect.* 40 (4) (1998) 257, [https://doi.org/10.1016/s0195-6701\(98\)90301-2](https://doi.org/10.1016/s0195-6701(98)90301-2).
- [32] R.V. Badhe, et al., Systemic toxicity eliciting metal ion levels from metallic implants and orthopedic devices - a mini review, *Toxicol. Lett.* 350 (2021) 213, <https://doi.org/10.1016/j.toxlet.2021.07.004>.
- [33] A.E.M. Hosny, et al., The increasing threat of silver-resistance in clinical isolates from wounds and burns, *Infect. Drug Resist.* 12 (2019) 1985, <https://doi.org/10.2147/IDR.S209881>.
- [34] A. Ordooei Javan, et al., A review on colistin nephrotoxicity, *Eur. J. Clin. Pharmacol.* 71 (7) (2015) 801, <https://doi.org/10.1007/s00228-015-1865-4>.
- [35] M.G. Habets, M.A. Brockhurst, Therapeutic antimicrobial peptides may compromise natural immunity, *Biol. Lett.* 8 (3) (2012) 416, <https://doi.org/10.1098/rsbl.2011.1203>.
- [36] L. Zhao, et al., Protein adsorption on TiO<sub>2</sub> nanostructures and its effects on surface topography and bactericidal performance, *Appl. Surf. Sci.* 576 (2022), <https://doi.org/10.1016/j.apsusc.2021.151779>.
- [37] Z. Maimaiti, et al., Host immune regulation in implant-associated infection (IAI): what does the current evidence provide us to prevent or treat IAI? *Bioengineering (Basel)* 10 (3) (2023) <https://doi.org/10.3390/bioengineering10030356>.
- [38] D.P. Pires, et al., Current challenges and future opportunities of phage therapy, *FEMS Microbiol. Rev.* 44 (6) (2020) 684, <https://doi.org/10.1093/femsre/fuaa017>.
- [39] J. Jurgens, Top 10 Emerging Technologies of 2023, *World Economic Forum*, 2023.
- [40] S.A. Strathdee, et al., Phage therapy: from biological mechanisms to future directions, *Cell* 186 (1) (2023) 17, <https://doi.org/10.1016/j.cell.2022.11.017>.
- [41] K.E. Kortright, et al., Arms race and fluctuating selection dynamics in *Pseudomonas aeruginosa* bacteria coevolving with phage OMK01, *J. Evol. Biol.* 35 (11) (2022) 1475, <https://doi.org/10.1111/jeb.14095>.
- [42] R. Wang, et al., Inhibition of *Escherichia coli* and *Proteus mirabilis* adhesion and biofilm formation on medical grade silicone surface, *Biotechnol. Bioeng.* 109 (2) (2012) 336, <https://doi.org/10.1002/bit.23342>.
- [43] A.S. Desislava Tzaneva, Nadezhda Petkova, Ventsislav Nenov, Albena Stoyanova, Panteley Denev Synthesis of carboxymethyl chitosan and its Rheological Behaviour in Pharmaceutical and Cosmetic Emulsions, *J. Appl. Pharmaceut. Sci.* (2017), <https://doi.org/10.7324/japs.2017.71010>.
- [44] J.E. Bean, et al., Triggered release of bacteriophage K from Agarose/Hyaluronan Hydrogel matrices by *Staphylococcus aureus* virulence factors, *Chem. Mater.* 26 (24) (2014) 7201, <https://doi.org/10.1021/cm503974g>.
- [45] J.A. Wroe, et al., Bacteriophage delivering hydrogels reduce biofilm formation in vitro and infection in vivo, *J. Biomed. Mater. Res.* 108 (1) (2020) 39, <https://doi.org/10.1002/jbm.a.36790>.
- [46] H. Huang, et al., Tissue-selective restriction of RNA editing of CaV1.3 by splicing factor SRSF9, *Nucleic Acids Res.* 46 (14) (2018) 7323, <https://doi.org/10.1093/nar/gky348>.
- [47] Y.J. Chuah, et al., Simple surface engineering of polydimethylsiloxane with polydopamine for stabilized mesenchymal stem cell adhesion and multipotency, *Sci. Rep.* 5 (2015) 18162, <https://doi.org/10.1038/srep18162>.
- [48] Y. Delaviz, et al., Infection resistant biomaterials, in: *Biomaterials and Medical Device - Associated Infections*, 2015, p. 223.
- [49] B.A. Castro, et al., Macrophage migration inhibitory factor downregulation: a novel mechanism of resistance to anti-angiogenic therapy, *Oncogene* 36 (26) (2017) 3749, <https://doi.org/10.1038/onc.2017.1>.
- [50] L. Wang, et al., <https://doi.org/10.1101/2023.10.26.564292>, 2023.
- [51] M. Dewor, et al., Macrophage migration inhibitory factor (MIF) promotes fibroblast migration in scratch-wounded monolayers in vitro, *FEBS Lett.* 581 (24) (2007) 4734, <https://doi.org/10.1016/j.febslet.2007.08.071>.
- [52] R.P. Verma, Titanium based biomaterial for bone implants: a mini review, *Mater. Today: Proc.* 26 (2020) 3148, <https://doi.org/10.1016/j.matpr.2020.02.649>.
- [53] H. Wunderlich, K.L. Kozielski, Next generation material interfaces for neural engineering, *Curr. Opin. Biotechnol.* 72 (2021) 29, <https://doi.org/10.1016/j.copbio.2021.09.005>.
- [54] W. Xuan, et al., Dualistic roles and mechanistic insights of macrophage migration inhibitory factor in brain injury and neurodegenerative diseases, *J. Cerebr. Blood Flow Metabol.* 43 (3) (2023) 341, <https://doi.org/10.1177/0271678X221138412>.
- [55] S. Song, et al., Macrophage migration inhibitory factor family proteins are multitasking cytokines in tissue injury, *Cell. Mol. Life Sci.* 79 (2) (2022) 105, <https://doi.org/10.1007/s00018-021-04038-8>.
- [56] A. Petrovic Fabijan, et al., Translating phage therapy into the clinic: recent accomplishments but continuing challenges, *PLoS Biol.* 21 (5) (2023) e3002119, <https://doi.org/10.1371/journal.pbio.3002119>.
- [57] L. Plumet, et al., Bacteriophage therapy for *Staphylococcus aureus* infections: a review of animal models, treatments, and clinical trials, *Front. Cell. Infect. Microbiol.* 12 (2022) 907314, <https://doi.org/10.3389/fcimb.2022.907314>.